Journal of Power Sources 255 (2014) 360–367

Contents lists available at ScienceDirect

Journal of Power Sources

journal homepage: www.elsevier.com/locate/jpowsour

A multi scale multi-dimensional thermo electrochemical modelling of high capacity lithium-ion cells

Abbas Tourani*, Peter White, Paul Ivey

Faculty of Engineering and Computing, Coventry University, Priory Street, Coventry CV1 5FB, UK

HIGHLIGHTS

- A multi-scale thermo electrochemical model for lithium ion cells is developed.
- The test results of two lithium ion chemistry are presented.
- Predict the temperature and current distribution across the surface of the cell.
- Compare the model and test results for the lithium ion cells.

ARTICLE INFO

Article history:
Received 23 September 2013
Received in revised form
23 December 2013
Accepted 7 January 2014
Available online 15 January 2014

Keywords:
Lithium-ion
Modelling
Thermo electrochemical
Electric vehicle
Temperature distribution

ABSTRACT

Lithium iron phosphate (LFP) and lithium manganese oxide (LMO) are competitive and complementary to each other as cathode materials for lithium-ion batteries, especially for use in electric vehicles. A multi scale multi-dimensional physic-based model is proposed in this paper to study the thermal behaviour of the two lithium-ion chemistries. The model consists of two sub models, a one dimensional (1D) electrochemical sub model and a two dimensional (2D) thermo-electric sub model, which are coupled and solved concurrently. The 1D model predicts the heat generation rate (Qh) and voltage (V) of the battery cell through different load cycles. The 2D model of the battery cell accounts for temperature distribution and current distribution across the surface of the battery cell. The two cells are examined experimentally through 90 h load cycles including high/low charge/discharge rates. The experimental results are compared with the model results and they are in good agreement. The presented results in this paper verify the cells temperature behaviour at different operating conditions which will lead to the design of a cost effective thermal management system for the battery pack.

1. Introduction

The niche market of the battery electric vehicle (BEV) is based on reducing the production cost. In order to reduce the cost by 50% by 2030, current and future chemical and control technologies must be successfully incorporated. Thermal management plays a vital role in the pursuit of this goal [1]. A medium range BEV with 30 kWh of electric energy had in 2011 a battery pack with a mass of 300 kg. This is expected to reduce to 180 kg by 2020 [2]. From the battery cost perspective, the battery cells currently cost \$400 kWh^{-1} however the battery pack is more than double that cost due to the complex thermal and electric management system required. Research and Development (R&D) is estimated to reduce the cost of the battery pack to \$300 kWh^{-1} by 2030 from the current \$1000 kWh^{-1} [3]. Most of the current R&D is on improving the energy density of BEV cells via new chemistries, rather than investigating thermal aspect of the cells. The development of new electrolytes, cathode and anode materials is the core of cell level studies [4–6]. The thermal characteristic behaviour of the battery cell is also investigated in different papers such as [7]. The majority of them studied small capacity cells (less than 10 Ah capacities) and ignored the temperature distribution of the cell. The cell dimensions in BEV application are more than 10 times those of the small capacity cells. Therefore, the temperature distribution should be considered in any thermal study.

The first step to design a cost effective thermal management system for the battery electric vehicles (BEV) is to understand the thermal behaviour of the battery cell as the main source of heat. Having reviewed thermal researches on the lithium-ion cell applied in BEV, it is observed that researchers studied the heat generation and heat transfer including accumulation and dissipation in different levels. Researchers who applied the first principle

* Corresponding author. Tel.: +44 (0) 247 765 7734.
E-mail address: tourania@coventry.ac.uk (A. Tourani).

0378-7753/$ – see front matter © 2014 Elsevier B.V. All rights reserved.
http://dx.doi.org/10.1016/j.jpowsour.2014.01.030

electrochemical models focused on the heat generation terms and left the heat dissipation part for the battery pack level study. On the other hand, researchers, who worked on the heat transfer study in batteries, assumed simply a resistive heating as the heat source in their heat transfer model and focused on the heat dissipation and temperature distribution through battery packs [8]. However, the thermal issues of the lithium-ion cells applied in EV have not been fully studied concurrently. This paper focuses on the thermal behaviour of the batteries in a BEV at the cell level. The model is a first principle model which accounts for operating temperature effect on the performance of the cell. In order to show the validity of the model results, the lithium-ion cells are experimentally investigated and the results are compared by the model results and the model results are in good agreement with the experimental measurements. Both aspects of the thermal study, heat generation and dissipation, are considered in the thermal modelling. The heat generation rate is calculated and the model is capable of studying the heat dissipation in 3D. The heat generation and dissipation rates are dependent variables and therefore the two models are coupled to detect more precisely the heat generation term and temperature distribution throughout the cell. Further, the cell component properties as available in the literature are function of temperature and state of charge and are incorporated in to the model.

2. The case studies

Lithium-ion batteries comprise a family of battery chemistries that employ various combinations of anode and cathode materials. Lithium iron phosphate (LFP) and lithium manganese oxide (LMO) are competitive and complementary to each other as cathode materials for lithium-ion batteries, especially for use in electric vehicles. LMO batteries have been used in electric tools and majority of on road electric cars such as Nissan Leaf use this type of the lithium-ion chemistry; LFP battery cell also uses in GM electric vehicle, Chevrolet Volt. However, the case studies in this paper are not representative of any particular electric cars and their typical data are given in Table 1. The case study battery cells have the pouch structure and are dedicated for electric vehicle applications. The fundamental configuration of the cells is shown in Fig. 1, which is not to scale and is for illustration purposes. The principle parts of the battery cell are negative electrode collector (Cu), negative electrode, separator, positive electrode and positive electrode collector (Al). This configuration repeats several times (about 10 times) and results in a battery thickness of approximately 7 mm (*Z*-direction).

3. The model definition

The electrochemical reactions in the battery cell are defined as heterogeneous reactions which means all of the reactions occur at interfaces between electrode, separator and electrode in *Z* direction, see Fig. 1. On the other hand, the high electronic conductivity of the current collectors (Al, Cu) bonded to the electrodes provide a high conductive electric layer which results in the reaction taking place in the *Z* direction. Hence, the 1D electrochemical model has been applied by the researchers who focus on the cell level study. Therefore, with a 1D electrochemical model, most of the reactions are determined without undue complexity [9]. This approach has proved to be a reliable approach for projects in which the component material improvement is not subject of the study.

Table 1
The battery cells data.

Parameters	Lithium iron phosphate (LFP)	Lithium manganese oxide (LMO)
Capacity (Ah)	19.6	20
Voltage (V)	3.3	4.2
Cell dimensions (mm)	7 × 160 × 227	8 × 177 × 240

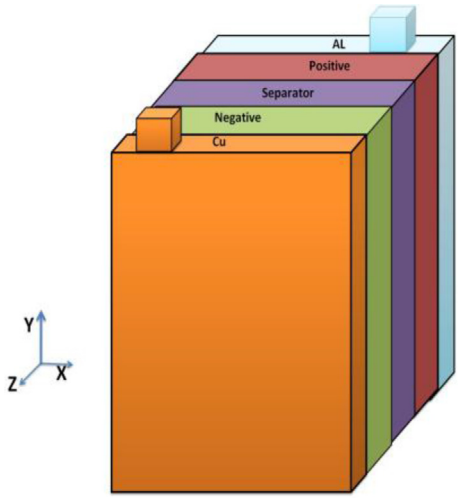

Fig. 1. The fundamental configuration of the battery cell.

The proposed model consists of two sub models, the 1D electrochemical sub model and 2D thermo-electric sub model, which are coupled and solved concurrently. The 1D model can predict the heat generation rate (*Qh*) and voltage (*V*) of the battery cell through different load cycles. The 2D thermo electric model of the battery cell accounts for temperature distribution and current distribution across the surface of the battery cell. The model from a numerical methods perspective is a finite element method and both 1D and 2D models are discretised into computational cells. In terms of sequence, the model input is a load cycle which is representative of the expected drawing down of power/current from the battery cell with time. The 1D electrochemical model for the load cycle, solves the mass transfer, charge balance and electric kinetic equations concurrently and predicts the voltage and state of charge for each components of the cell (collectors, electrodes and electrolyte). The voltage at a point in the 1D model which corresponds to the tab in the battery cell is then mapped to the tab position in the 2D thermo electric model. This is in contrast with the Gerver [10] combined model which is composed of a grid of 1D electrochemical models coupled to a thermal model and a 2D resistor network to determine current and temperature distributions in 3D dimensions. However,

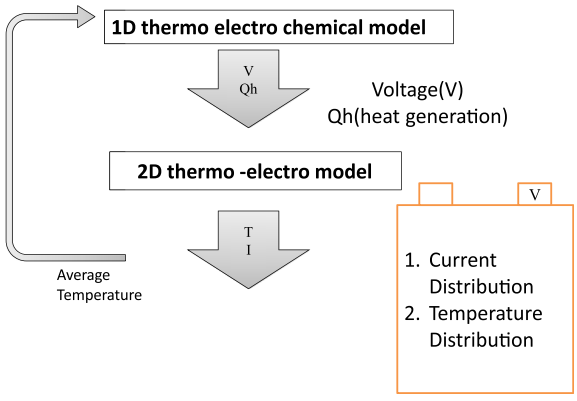

Fig. 2. The model sequence.

based on the input from 1D mode that are the tab voltage and a volumetric heat generating term, the 2D model predicts temperature and current for each computational cells and then weight average of the temperature across the surface is mapped to the 1D model and the loop is repeated till the solution converges. See Fig. 2.

In addition, the associated total heat generation rate which includes reversible (reaction) and irreversible (Ohmic and over potential terms), maps to each computational cell in the 2D thermo electric model, and the 2D model solves the charge balance (Joule equation) and energy equation concurrently. Hence it has an extra benefit of accounting for the Ohmic losses across the surface area of the cell which cannot be neglected in battery cells with large surface area such as EV cells. This is in contrast with the battery model released along with COMSOL Multiphysics 4.2© and widely was used by other researchers such as Xiao and Choe [11] in which only a volumetric heat generation term is applied.

3.1. The 1D electrochemical sub model

The 1D electrochemical sub model is based on Doyle model [12] which has been built by COMSOL4.a©. The model was developed by White et al. to include thermal effects [1]. Bernadi et al. applied the model to analyse the relaxation behaviour in cells designed for hybrid vehicle propulsion [13]. It solves six coupled, nonlinear equations to calculate the cell voltage and current as a function of time, and to calculate the potentials in the electrolyte and electrode phases, salt concentration, intercalated lithium concentration, reaction rate, and current density in the electrolyte as functions of time and position within the cell.

The charge balance $\varnothing_l$ in the solid phase is governed by the Ohm's law.

$$\nabla\left(-k_1^{\text{eff}}\nabla\varnothing_l\right) = -S_a j_{\text{loc}} \tag{1}$$

k_l is the electronic conductivity, j_{loc} is the local charge transfer current density (positive for anodic reactions) (A m^{-2}), S_a is the specific surface area (m^2 m^{-3}). The ionic charge balance for the liquid phase expresses as:

$$\nabla\left\{-k_2^{\text{eff}}\nabla\varnothing_2 + \frac{2RTk_2^{\text{eff}}}{F}\left[1+\frac{\partial \ln f}{\partial \ln c_2}\right][1-t_+]\nabla(\ln c_2)\right\} = S_a j_{\text{loc}} \tag{2}$$

The subscripts 1 and 2 denote to the solid and liquid phases of active materials. In the Doyle model, the mass balance of lithium ions in an intercalation particle of electrode active material is described by Fick's law. This is expressed as follows by introducing the dimensionless radius, $y = r/r_p$, where r_p is the particle radius, D_1 solid phase diffusivity, and c_1 is the concentration of lithium in the active material.

$$y^2 r_p \frac{dc_1}{dt} + \partial\left(-y^2\frac{D_1}{r_p}\frac{\partial c_1}{\partial y}\right) = 0 \tag{3}$$

The material balance for the binary electrolyte in the liquid phase is given by:

$$\varepsilon_2\frac{dc_2}{dt} + \nabla\left\{-D_2^{\text{eff}}\nabla c_2 - \frac{i_2}{F}(1-t_+)\right\} = 0 \tag{4}$$

c_2 is the cation concentration in electrolyte, ε denotes the porosity (volume fraction of electrolyte), and D_2^{eff} the effective diffusivity in the electrolyte. Butler–Volmer equation describes the electrode kinetics.

$$j_{\text{loc}} = i_o\left\{\exp\left(\frac{\eta F}{RT}\right) - \exp\left(-\frac{\eta F}{RT}\right)\right\} \tag{5}$$

where

$$\eta = \phi_1 - \phi_2 - E_{\text{ref}}(c_1,\ \text{surf}) \tag{6}$$

$$i_0 = k_0\sqrt{c_2\left(c_{1,\max} - c_{1,\ \text{surf}}\right)c_{1,\ \text{surf}}} \tag{7}$$

i_0 denotes the exchange current density, and E_{ref} refers to the electrode equilibrium potential of particle, which is a function of the concentration at the particle surface, c_1^{surf}. In addition, k_0 denotes the reaction rate constant, and $c_{1,\max}$ is the maximum surface concentration. The activation over potential, η, for all electrode reactions in the electrode receives an extra potential contribution.

3.2. Temperature dependency of parameters

One of the accepted formulae for temperature dependence of reaction rate is the Arrhenius equation. [1,14] The Arrhenius equation is best seen as an empirical relationship and is used to model the temperature variation of diffusion coefficients and many other parameters [15]. However, measured correlations for some parameters also proposed [16]. The lithium-ion cell parameters, temperature and concentration dependence equations of electrolyte conductivity, salt diffusivity and thermodynamic factor are taken from Ref. [17]. The diffusivity of negative electrode is temperature dependent and is given by Ref. [7].

- Electrolyte conductivity (k_l):

$$\begin{aligned} k_l = {} & 0.0001c_1\Big(-10.5 + 0.668\times10^{-3}c_1 + 0.494{*}10^{-6}c_1^2 \\ & +0.074T - 1.78\times10^{-5}c_1\times T - 8.86\times10^{-10}c_1^2\times T \\ & - 6.96\times10^{-5}T^2 + 2.8\times10^{-8}c_1\times T^2\Big)^2 \end{aligned} \tag{8}$$

- Electrolyte salt diffusivity:

$$D_l = 10^{-4}\times10^{-4.43-\left(\frac{54}{T-229-5\times10^{-3}cl}\right)-0.22\times10^{-3}cl} \tag{9}$$

- Activity dependence:

$$\begin{aligned} \frac{\partial \ln f}{\partial \ln c1} = {} & \Big(0.601 - 0.24\left(10^{-3}cl\right)^{0.5} + 0.982(1 \\ & - 0.0052(T-294))\left(10^{-3}cl\right)^{1.5}\Big) \end{aligned} \tag{10}$$

- Negative electrode intercalation diffusivity:

$$D_{\text{Sn}} = 1.4523\times10^{-13}\exp\left(\frac{68025.7}{8.314472}\left(\frac{1}{318}-\frac{1}{T}\right)\right) \tag{11}$$

Table 2
The 2D model parameters.

	Z (μm)	X (mm)	Y (mm)	Density (g cm^{-3})	Heat capacity (J gK^{-1})	Thermal conductivity (W mK^{-1})		Electric conductivity (S m^{-1})
Positive collector	20	177	240	2.7	0.9	238		3.83E+07
Positive electrode	150	177	240	1.5	0.7	5		139
Negative collector	10	177	240	8.96	0.385	398		6.33E+07
Negative electrode	145	177	240	2.5	0.7	5		100
Separator	52	177	240	1.2	0.7	1		f(DOD,T) < 1.5
Equivalent parameters								
Thermal conductivity:				2.14	0.678	λ_x	27.23	f(DOD,T)
In X,Y direction parallel						λ_y	27.23	
In Z direction series						λ_z	3.39	

3.3. Energy equation

The thermodynamics of the cell is based on the thermal energy balance over an elementary volume in a battery. The differential equation that describes temperature distribution in the battery takes following conservation form

$$\rho c_p \frac{\partial T}{\partial t} = \lambda \nabla^2 T + q_g - q_d \tag{12}$$

q_d is the rate of heat exchanges between the battery cell and surroundings.

$$q_d = \frac{hA_{cell}}{V_{cell}}(T - T_s) \tag{13}$$

h is the heat transfer coefficient (W m^{-2} K^{-1}), T is the cell temperature and T_s is the surrounding temperature. A_{cell} and V_{cell} are the surface area and volume of the battery cell.

The heat source term (q_g) in the battery cell is defined by Ref. [18]

$$q_g = \sum_j a_{sj} i_{nj} (\varnothing_s - \varnothing_e - U_j) + \sum_j a_{sj} i_{nj} T \frac{\partial U_j}{\partial T} + \sigma^{eff} \nabla \varnothing_s \nabla \varnothing_s + k^{eff} \nabla \varnothing_e \nabla \varnothing_e + k_D^{eff} \nabla \ln c_1 \nabla \varnothing_e \tag{14}$$

The first term on the right hand side is potential deviation in the control volume from the equilibrium potential (irreversible heat). The second term represents the entropic effects (reversible heat). The third term shows the Ohmic heat in the solid phase and the last two terms represents the Ohmic heats in the solution phase.

3.4. The 2D thermo-electro model

The 2D model is an equivalent model representing the 3D geometry of the battery cell and the thermal and electrical properties of the material are used to calculate the equivalent properties. The 2D mode parameters are given in Table 2. The battery properties in the X and Y directions are considered to be in parallel and in the Z direction is series. See Fig. 1 for direction. The battery is a layered cell containing multiple materials with different thicknesses and thermal properties. See Fig. 1. As a result, the thermal conductivity of the battery is anisotropic. The composite charge conductivity is calculated as follows

$$k = \left(\frac{l_a}{k_a} + \frac{l_c}{k_c} + \frac{RT}{i_{0,a} nF} + \frac{RT}{i_{0,c} nF} \right)^{-1} \tag{15}$$

The heat flows perpendicular to the X direction and flows through each sheet in series, while heat flowing along the stack flows through each layer in parallel. Because the thickness of each layer is very small, significant computational time is consumed when attempting to resolve heat flowing in each layer. Instead, the battery unit cell is typically modelled as a uniform layer with anisotropic thermal conductivity and uniform heat generation as follows:

Thermal conductivity in X and Y direction (l_i denotes the thickness of layer i):

$$\lambda = \frac{\sum \lambda_i l_i}{\sum l_i} \tag{16}$$

Thermal conductivity in z direction

$$\lambda_z = \sum \frac{l_i}{\sum \frac{l_i}{\lambda_i}} \tag{17}$$

The heat capacity for the equivalent cell is volume averaged as follows

$$\rho C_p = \sum (\rho C_p)_i l_i / \sum l_i \tag{18}$$

3.5. Thermal boundary condition

The battery cells are studied to determine the cells behaviour in the absence of any active cooling system. The boundary condition has a significant effect on the temperature distribution of the cell. The experiment and the model in this project are set up in a same way. The ambient temperature is measured in the test and used as the surrounding temperature (T_s) in the model, equation (13). The cell during the test was placed vertically in a condition without having any conductive heat transfer with the surrounding. In the model, a heat transfer coefficient, h, is considered. The heat transfer coefficients for all surfaces of the cell are considered as a constant number equal to 6 W m^{-2} K^{-1} [1,19]. This number is obtained by calculating the Nusselt number of the buoyancy flow around the cell. However, the model is capable to set up different heat transfer boundary conditions and is used to study different heat transfer coefficients and ambient conditions.

4. The experimental measurements

The high capacity battery cells, 20 Ah, at different load cycles are examined. Three battery cells with the same specification are tested concurrently and shown that the test results are repeatable. To ensure the validity of the test results, the uncertainty and level of confidence of the test results are calculated and compared to the equipment accuracy. Three fundamental measurements, temperature, terminal voltage and current throughout the load cycle are measured. The parameters are typically measured at periodic

intervals during a battery test sequence. The 15 thermocouples are set as a grid across the surface of the cells to measure the temperature. The tests are performed at ambient temperature which is also monitored throughout the tests. In order to have repeatable results, three battery cells with the same specification, chemistry and construction are tested concurrently. In this project, data acquisition intervals of 4 s were applied and the sample data reviewed carefully to be sure that all samples are independent.' See Fig. 3.

Inverse Distance Weighting (IDW) method [20] is used to plot temperature contours from thermocouples data. The IDW method estimates the values of an attribute by using a linear combination of values at sampled points weighted by an inverse function of the distance from the point of interest to the sampled points. In addition, a thermal camera is applied to detect hot spots and the temperature distribution on the surface of the battery cells. The two set of experiment results, thermocouple data and the thermal image, show the same gradient across the sample's surface and identified the hot zone on the sample.

Fig. 3. The test set up.

5. Results and discussion

The cells are tested with a load cycle lasting 90 h with range of constant current charge and discharge rates from 0.2C (0.2 times nominal current that is 20 A) to 10C. See Fig. 4. The cell voltage and current were acquired for each time step, 4 s. Temperature over the surface of the cell was measured by 15 Thermocouple probes with their distribution on the cell surface shown in Fig. 3.

The same load cycle is applied for the model and test. The model prediction for average temperature of the LFP cell surface and the measured average temperature are illustrated in Fig. 5. In the model it is assumed that convection was from the large plane cell surfaces with a heat transfer coefficient of $h = 6\ \mathrm{W\ m^{-2}\ K^{-1}}$ [19], and an ambient temperature which is constant and equal to 20 °C. Fig. 5 shows the model prediction is in good agreement with the measurement data especially in high current charge/discharge rates (bigger than 1C). For example, the cell after a 10 min discharge with 5C (100 A) reaches a temperature of 45 °C and the corresponding temperature for the model in this condition is 45.5 °C. In addition, the temperature drops and reaches the ambient temperature at the same time in both the model and the test data.

There is a subtle difference between the predicted temperature and the experimental data during the charge/discharge process with the rate (less than 1C), see Fig. 5. For example, the model predicts temperature of 28 °C for 1C discharge rate which is 4° lower than that measured in the test. However, the difference is minimum at the peak point and the model reaches the ambient temperature at the same time and this is important as it shows that the model thermal mass compensates for the difference in prediction of the peak value. The LFP cell study shows that the predicted temperature in low charge/discharge rate (less than 1C) are not as good as high rate in agreement with the experimental data. The difference between heat generation terms in low and high current rate could contribute to make the difference between the predicted and measured temperature. In high current rate, the irreversible term dominates the other heat generation terms and the Ohmic term in the model correctly represents the Ohmic heat in the battery cell. In the low current, the reversible term which is the sum of producible reversible work and entropic heating from the reaction contributes more on the generated heat. The model's predicted reversible heat is not the right representative of reversible heat which occurred during the measurement. This hypothesis is verified by conducting another set of experimental measurement with different lithium-ion chemistry. Therefore, a lithium manganese oxide battery (LMO) cell is selected for further study which is explained in the flowing section.

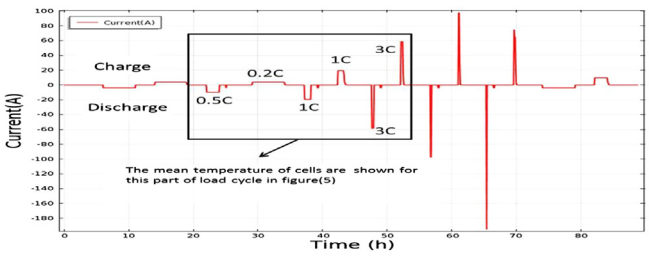

Fig. 4. The LFP test/model load cycle.

The LMO battery cell which is chosen for the study has the same capacity as the LFP cell, 20 Ah. Fig. 6 shows the model prediction for average temperature of the LMO cell surface and the measurement of average temperature. In the model it is assumed that convection was from the large plane cell surfaces with a heat transfer coefficient of $h = 6\ \mathrm{W\ m^{-2}\ K^{-1}}$ [19], and an ambient temperature which is considered by the measured ambient temperature throughout the test. As it can be seen in Fig. 7, the model voltage prediction is in good agreement with the measurement either high or low current discharge rates. The electrochemical model can provide the polarisation curve in the accuracy of 95%. In addition, temperature dependent parameters and the heat generation and dissipation terms considered in the model predict the average temperature with the accuracy 93%. The measured temperature and predicted rise considerably over the discharge period with the same trend.

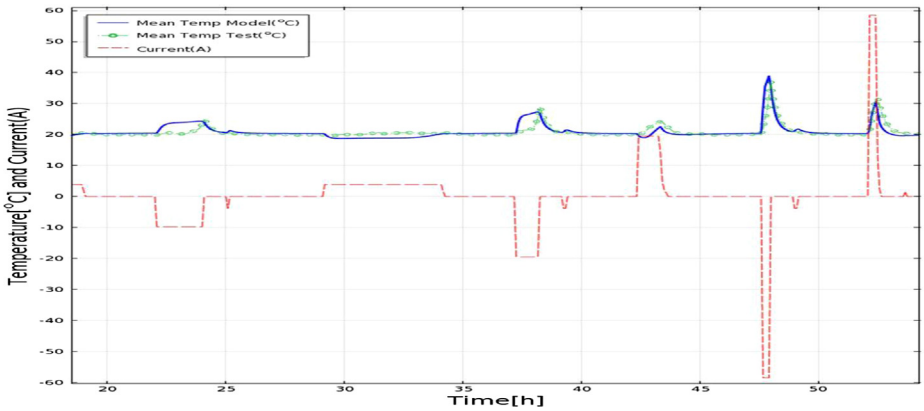

Fig. 5. Comparison between mean temperature of the model result (LFP cell) and the test.

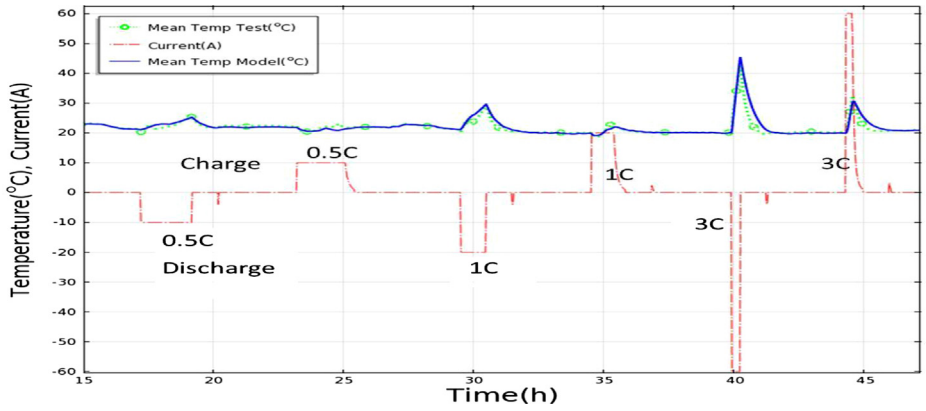

Fig. 6. Comparison between mean temperature of the model result (LMO cell) and the test.

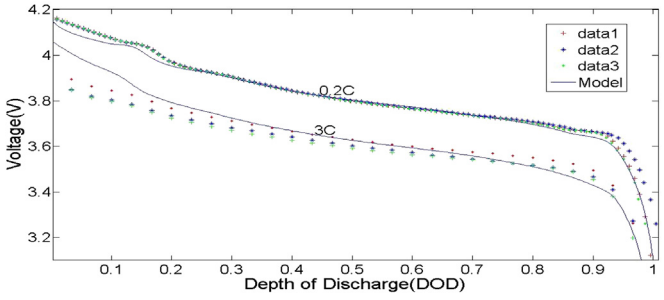

Fig. 7. Voltage curves for the LMO cell at different discharge rates (1C = 20 Ah).

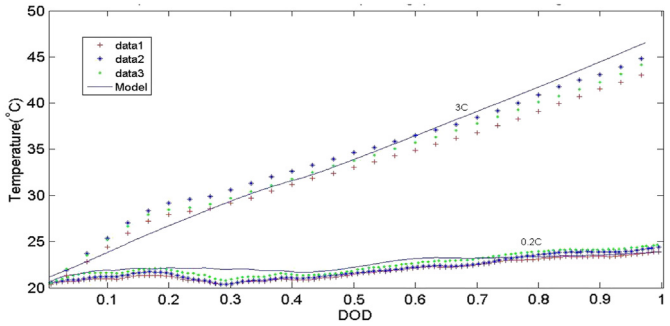

Fig. 8. Mean temperature variation with depth of discharge for the LMO cell at different discharge rates (1C = 20 Ah).

However, the measured temperature jump and fall 5% when the cell 20% is discharged which is not seen in the model especially for high currents rates. See Fig. 8.

The results demonstrate that at low current rates (0.2C), the LMO cell performance is better in terms of maintaining the voltage during discharge. These low current rates would correspond to cell use in EV whilst the high discharge rates are associated with use in hybrid vehicles, and hence a short life.

In order to obtain the temperature distribution across the cell surface, thermocouples data and thermal camera are used. The predicted temperature contours across the surface of the cell are compared with the thermal camera image at 3C discharge; Fig. 9. It shows that both, thermal camera and the model prediction, determine the same pattern for the temperature distribution across the surface of the cell. Overall the temperature difference across the cell at the end of discharge is about 2 °C and this corresponds to drawing 60 A current from the cell for 20 min. The maximum temperature occurs at the top of the cell near the tabs and the contours are symmetric. However, the temperature contour depends on how set up the thermal boundary condition. In the presented results, it is assumed that the heat dissipates from the edges and surfaces which is an appropriate estimation for natural convection based on buoyancy flow and calculating Nusslet number [19]. Temperature and voltage distributions are analogues [21], and thus the contours on Fig. 8 represent voltage distribution across the cell as well.

6. Conclusion

A multi scales physics based model is developed to study the battery cell behaviour and the model results are compared by the

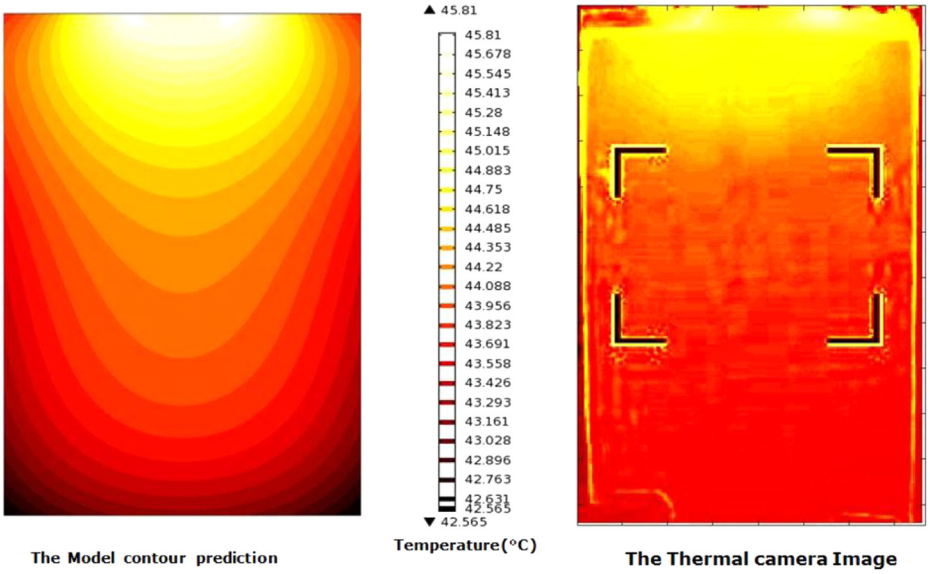

Fig. 9. Comparison between temperature contour of the model result and the test.

experimental results. The model voltage prediction is in agreement with the measurement either high or low current discharge rates. The electrochemical model can provide the polarisation curve in the accuracy of 95%. In addition, the model predicts the average temperature with the accuracy 93%.

Two different lithium chemistries are applied and the results show the model can predict the temperature and voltage of lithium polymer cell (LMO) more accurate than for the lithium iron phosphate (LFP) cell. The study results show the LFP cell parameters' dependency functions should be obtained experimentally or the functions should be adapted to apply for high capacity cells as most of them have not been applied for EV application.

For BEV which operates at a nominal low current rate, the order of magnitude of heat source through the cell is less than 850 W m^{-3} during discharge process; this amount of heat can be managed to keep the cell at desired operating temperature. BEV battery is more likely encounter problems to keep it warm at the low end of the temperature range, than to require cooling at high ambient temperature. The temperature difference across the cell at the end of discharge is about 2 °C and this corresponds to drawing 60 A current from the cell for 20 min in ambient temperature of 20 °C. The maximum temperature occurs at the top of the cell near the tabs and the contour pattern depends on the boundaries' heat transfer condition.

It is recommended to study the battery cell thermal behaviour in typical and realistic driving cycles, continue the concurrent study of heat generation and dissipation in EV batteries pack level and compare performance of thermal management techniques to maintain the cell in the desired operating temperature in terms of lightweight and less sophisticated cooling systems.

List of symbols

c_1	concentration of the electrolyte (mol m^{-3})
c_s	surface concentration in spherical particle (mol m^{-3})
C_p	specific heat (J kg^{-1} K^{-1})
j_{loc}	transfer current density (A m^{-2})
q	volumetric heat generation rate (J m^{-3} s^{-1})
U_j	equilibrium potential (V)
k^{eff}	effective solution conductivity (1 (Ωm)$^{-1}$)
λ	thermal conductivity (W m^{-1} K^{-1})
ρ	density (kg m^{-3})
σ_{eff}	effective matrix conductivity (1 (Ωm)$^{-1}$)
ϕ_1	potential in the matrix phase (V)
ϕ_2	potential in the solution phase (V)
k	electronic conductivity (S m^{-1})
S_a	specific surface area (m^2 m^{-3})
R	gas constant (8.3143 J mol^{-1} K^{-1})
y	fraction of lithium in the positive electrode
γ	Bruggeman coefficient
l_c	thicknesses of cathode electrode (m)
T	temperature (K)
F	Faraday's constant (96487 C mol^{-1})
f	ionic activity coefficient
t_+	transport number
ε	porosity (volume fraction of electrolyte)
D_l^{eff}	effective diffusivity in the electrolyte (m^2 s^{-1})
i_0	exchange current density (A m^{-2})
E_{ref}	electrode particle's equilibrium potential (V)
$c_{1,\,surf}$	particle surface concentration (mol m^{-3})
k_0	reaction rate constant
$c_{1,max}$	maximum surface concentration (mol m^{-3})
η	activation overpotential (V)
D_1	electrolyte salt diffusivity (m^2 s^{-1})
$\partial ln\ f/\partial ln\ c1$	activity dependence
D_{sn}	Negative electrode intercalation diffusivity (m^2 s^{-1})
U_{ref}	open potential of the electrode (V)
x	fraction of lithium in the negative electrode
l_a	Thicknesses of anode electrode (m)

Appendix 1. The electrochemical model equations

$$k_i^{eff} = k_i\,\varepsilon^{\gamma} \quad ,i = 1,2 \tag{A-1}$$

$$D_i^{eff} = D_i\,\varepsilon^{\gamma} \quad ,i = 1,2 \tag{A-2}$$

From Ref. [22]

$$U_{ref,n} = -0.16 + 1.32\exp(-3x) + 10\exp(-2000x) \tag{A-3}$$

From Ref. [23]

$$U_{\mathrm{ref,LMO}} = -23.53y^5 + 52.43y^4 - 44.86y^3 + 18.4y^2 - 3.35y + 3.16 \tag{A-4}$$

From Ref. [16]

$$\left(\frac{\mathrm{d}U}{\mathrm{d}T}\right)_n = 344.1347148\exp(-32.9633287x + 8.316711484)/(1 + 749.0756003\exp(-34.7909964x + 8.887143624)) - 0.8520278805x + 0.36229929x^2 + 0.2698001697 \tag{A-5}$$

$$\left(\frac{\mathrm{d}U}{\mathrm{d}T}\right)_{\mathrm{LMO}} = \Big(4.131274309\exp(0.571536523y) + 1.281681122\sin(-4.9916739y) - 0.090453431\sin(-20.9669665y + 12.5788250) - .0313472974\sin(31.7663338y - 22.4295664) - 4.14532933 + 8.147113434y - 26.064581y^2 + 12.7660158y^3 - 0.184274863 \times \exp(-(y - 0.5169435168)/0.04628266783)^2\Big) \tag{A-6}$$

From Ref. [10]

$$U_{\mathrm{ref,LFP}} = -5.76 \times 10^3 y^4 + 2.07 \times 10^4 y^3 - 2.79{*}10^4 \times y^2 + 1.67 \times 10^4 y - 3.77 \times 10^3 \tag{A-7}$$

$$\left(\frac{\mathrm{d}U}{\mathrm{d}T}\right)_{\mathrm{LFP}} = -0.35376y^8 + 1.3902y^7 - 2.2585y^6 + 1.9635y^5 - 0.98716y^4 + 0.28857y^3 - 0.046272y^2 + 0.0032158y - 1.9186 \times 10^{-5} \tag{A-8}$$

References

[1] L. Cai, R.E. White, in: Proceedings of the COMSOL Conference, 2009.
[2] P. Harrop, R. Das, Car Traction Batteries – the New Gold Rush 2010–2020, IDTechEx Ltd, 2009.
[3] The Climate Group, Breaking the Deadlock Technology for a Low Carbon Future, July 2009.
[4] K.H. Kwon, C.B. Shin, T.H. Kang, C. Kim, J. Power Sources 163 (2006) 151–157.
[5] Y. Ma, H. Teng, M. Thelliez, SAE Int. J. Eng. 3 (2010) 306–317.
[6] S.C. Nagpure, R. Dinwiddie, S.S. Babu, G. Rizzoni, B. Bhushan, T. Frech, J. Power Sources 195 (2010) 872–876.
[7] S.C. Chen, C.C. Wan, Y.Y. Wang, J. Power Sources 140 (2005) 111–124.
[8] G. Guo, B. Long, B. Cheng, S. Zhou, P. Xu, B. Cao, J. Power Sources 195 (2010) 2393–2398.
[9] G. Kim, S. Kandler, in: 4th International Symposium on Large Lithium Ion Battery Technology and Application, 2008.
[10] R.E. Gerver, J.P. Meyers, J. Electrochem. Soc. 158 (2011) A835–A843.
[11] M. Xiao, S. Choe, J. Power Sources 218 (2012) 357–367.
[12] M. Doyle, J. Newman, A.S. Gozdz, C.N. Schmutz, J.- Tarascon, J. Electrochem. Soc. 143 (1996) 1890–1903.
[13] D.M. Bernardi, J. Go, J. Power Sources 196 (2011) 412–427.
[14] K.J. Laidler, Chemical Kinetics, third ed., Harper & Row, Prentice Hall, 1987, p. 42.
[15] K. Smith, C. Wang, J. Power Sources 160 (2006) 662–673.
[16] V. Srinivasan, C.Y. Wang, J. Electrochem. Soc. 150 (2003).
[17] L.O. ValÃen, J.N. Reimers, J. Electrochem. Soc. 152 (2005) A882–A891.
[18] L. Rao, J. Newman, J. Electrochem. Soc. 144 (1997) 2697–2704.
[19] F.P. Incropera, Fundamentals of Heat and Mass Transfer, fourth ed., Wiley, 1996.
[20] D. Shepard, in: 68 Proceedings of the 1968 23rd ACM National Conference, 1968, pp. 517–524.
[21] J.R. Simonson, Engineering Heat Transfer, second ed., Palgrave Macmillan, 1988.
[22] L. Cai, Y. Dai, M. Nicholson, R.E. White, K. Jagannathan, G. Bhatia, J. Power Sources 221 (2013) 191–200.
[23] C. Wang, A.M. Sastry, J. Electrochem. Soc. 154 (2007) A1035–A1047.